UC Berkeley

Title
System reliability approach for rock scour

Permalink

Authors
George, Michael F
Sitar, Nicholas

Publication Date

DOI

System reliability approach for rock scour

Michael F. George*, Nicholas Sitar

Department of Civil and Environmental Engineering, University of California, Berkeley, USA

*Correspondence to: Department of Civil and Environmental Engineering University of California, Berkeley, CA 94720 USA. E-mail address: mike.george@berkeley.edu (M.F. George)

Abstract

Removal of individual blocks of rock is one of the principal mechanisms by which scour can occur, and prediction of block erodibility can be complicated due to the inherent variability associated with the rock mass as well as flow conditions in the vicinity of the block(s) in question. In order address the stochastic nature of the problem, we present a methodology for system reliability assessment of the probability of scour of 3D rock blocks subject to hydraulic loads within a block theory framework. Monte Carlo simulations are used to determine overall block failure probability, and to identify the most likely failure mode. A first-order reliability method (FORM) is then used to determine sensitivity to the different variables and hence the relative level of importance of the physical parameters with respect to the dominant failure mode. An example problem is used to illustrate the value of this information in focusing site investigations and analyses on the most important variables as well as in guiding decisions regarding scour mitigation strategies.

Keywords: Rock scour, Probability, Block theory, Monte Carlo, FORM

1. Introduction

Scour of rock is an issue for critical infrastructure such as dams, bridges and tunnels, where excessive erosion of the structure's foundation can compromise stability, leading to high remediation costs or even loss of life should catastrophic failure occur. Accordingly, reliable quantification of rock erodibility is necessary to ensure the continued, safe operation of these structures. The removal of individual blocks of rock by hydraulic forces is one of the primary mechanisms by which rock scour can occur. Prediction of block erodibility, however, is hindered by the inherent variability associated with the rock mass comprising the foundation/spillway as well as with flow conditions in the vicinity of the block.

To account for this variability, a system reliability approach for block stability is implemented. In recent years, risk and reliability methods have seen increased use among practitioners and researchers for quantification of event failure probability to aid in hazard analysis and the decision-making process. However, these studies have had limited use in the current state-of-the-art rock scour prediction models, e.g., Refs. 1–3. Reliability methods have been successfully applied to general rock slope stability in 2D,[4] and for 3D rock wedges defined by two discontinuity planes in Refs. 5– 7. We extend

the systems reliability approach to 3D rock blocks bound by three discontinuity planes and one free face. While the analysis is presented for hydraulic loading by channel flow, the method can be readily applied to block stability problems of similar geometry with other loading conditions (e.g., gravity, seepage, overtopping jet).

2. Model formulation

Material properties and processes in most geologic settings are inherently variable and accordingly a probabilistic approach is a natural choice for their evaluation. Quantification of the rock scour process requires a joint assessment of the erosive capacity of water and the resistive capacity of the rock mass. Variability in erosive capacity is predominantly produced by unsteadiness and turbulent flow conditions, which can change both spatially and temporally; while variability in rock block resistance is dominated by the spacing, orientation and shear strength (friction and dilation angle) of the discontinuities bounding the block (Fig. 1).
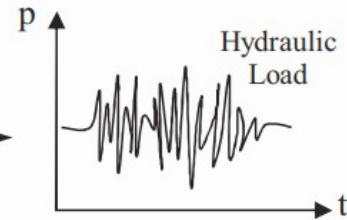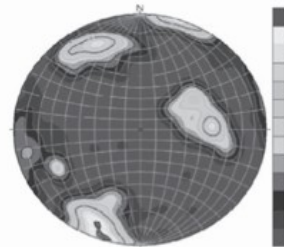
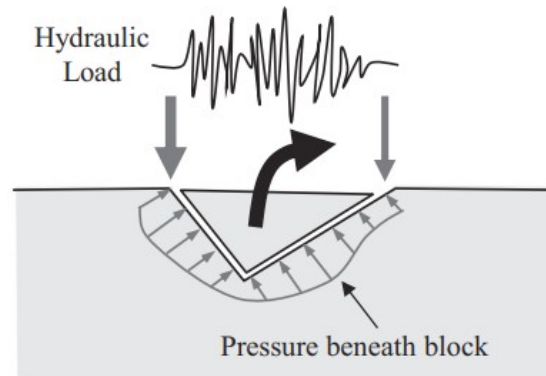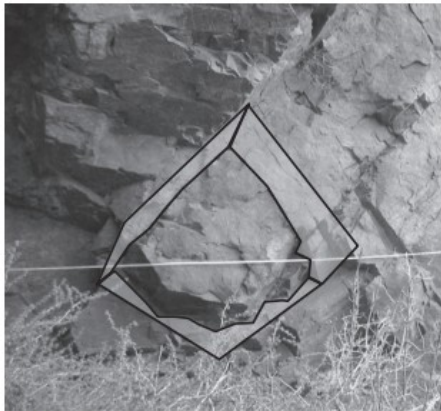**Fig.1.** Variability in the rock scour process.

Fig. 2. Rock block as defined by surrounding discontinuities (left) and schematic for block removal due to transmission of hydraulic pressures beneath block (right).

Removal of individual blocks of rock is one of the principal mechanisms by which scour occurs in unlined rock channels/ tunnels, bridge foundations, dam abutments, and plunge pools. The discontinuities around the block allow for transmission of hydraulic pressures to the block faces that can result in removal (failure) (Fig. 2). For 3D blocks, there are a number of kinematic failure modes that lead to a block being removed from its mold.[8] These consist of pure translational movements (e.g., lifting, oneplane sliding, or two-plane sliding), pure rotational movements (e.g., about an edge, about a corner, or about an arbitrary point), or some combination of translation and rotation (Fig. 3).

Failure of a removable block[9] in a particular failure mode is subject to several kinematic constraints that must be satisfied for a block to be eroded. For tetrahedral rock blocks, the number of kinematic failure modes and the

probability that the block is removable and rotatable is fairly low[10] since the number of failure planes is limited to 3. Accordingly, for the example analysis presented below, we only consider the pure translational modes (lifting, 1-plane sliding, and 2-plane sliding).

For pure translation modes, lifting of a block is kinematically feasible when

$$\mathbf{s} \cdot \mathbf{v}_i > 0, \text{ for all } i \tag{1}$$

where $\mathbf{s}$ is the direction of block movement (equal to the direction of the active resultant, $\mathbf{r}$, for lifting), and $\mathbf{v}_i$ is the block-side normal vector for the ith joint plane. **Bold** font signifies a vector/matrix quantity. This condition ensures the block moves away (lifts) from each of the bounding joint planes. The block-side normal may be

$$\mathbf{n}_i = \begin{bmatrix} \sin(\delta_i) \cdot \sin(\theta_i) \\ \sin(\delta_i) \cdot \cos(\theta_i) \\ \cos(\delta_i) \end{bmatrix},$$

$$\mathbf{v}_i = \mathbf{n}_i \text{ (block is above } i\text{th joint plane), or}$$

$$\mathbf{v}_i = -\mathbf{n}_i \text{ (block is below } i\text{th joint plane),} \tag{2}$$

where $\mathbf{n}_i$ is the upward normal for the ith joint plane and δ_i, θ_i are the dip and dip direction, respectively, of the ith joint plane. For block sliding on plane i only, the sliding direction is given by:

$$\mathbf{s} = \mathbf{s}_i = \frac{(\mathbf{n}_i \times \mathbf{r}) \times \mathbf{n}_i}{|\mathbf{n}_i \times \mathbf{r}|} \tag{3}$$

This is the orthographic projection of the active resultant force vector, $\mathbf{r}$, onto the sliding plane. Kinematic feasibility of 1-plane sliding is subject to the following constraints:

$$\mathbf{v}_i \cdot \mathbf{r} \leq 0, \text{ and}$$

$$\mathbf{s}_i \cdot \mathbf{v}_j > 0 \text{ for all } j \neq i, \tag{4}$$

where j represents the remaining two joint planes. The first condition ensures a component of the resultant is projected onto the plane of sliding, while the second guarantees the block is being lifted from the remaining joint planes. For block sliding on planes i and j simultaneously, the sliding direction is given by:

$$\mathbf{s} = \mathbf{s}_{ij} = \frac{\mathbf{n}_i \times \mathbf{n}_j}{|\mathbf{n}_i \times \mathbf{n}_j|} \cdot sign\left[(\mathbf{n}_i \times \mathbf{n}_j) \cdot \mathbf{r} \right], \tag{5}$$

where sign(·) is a function that returns 1 if "(·)" is positive and –1 if "(·)" is negative. The sliding direction is along the line of intersection between the two planes. The *sign* function determines which direction sliding occurs along this line considering the orientation of the active resultant. Kinematic feasibility of two-plane sliding on planes *i* and *j* is subject to the following constraints:

$$\mathbf{s}_{ij} \cdot \mathbf{v}_k > 0, \text{ and}$$
$$\mathbf{s}_i \cdot \mathbf{v}_j \leq 0, \text{ and}$$
$$\mathbf{s}_j \cdot \mathbf{v}_i \leq 0, \tag{6}$$

where *k* represents the remaining joint plane from which the block is lifted. The first condition ensures the block slides away from joint plane *k*. The second condition ensures the direction of block sliding on plane *i* is towards plane *j*, while the third condition ensures the direction of sliding on plane *j* is towards plane *i*.

| Lifting | Sliding (1 plane) | Sliding (2 planes) |

Pure Translations

| Rotation (edge) | Rotation (corner) | Slumping | Torsional Sliding |

Pure Rotations   Rotation + Translation

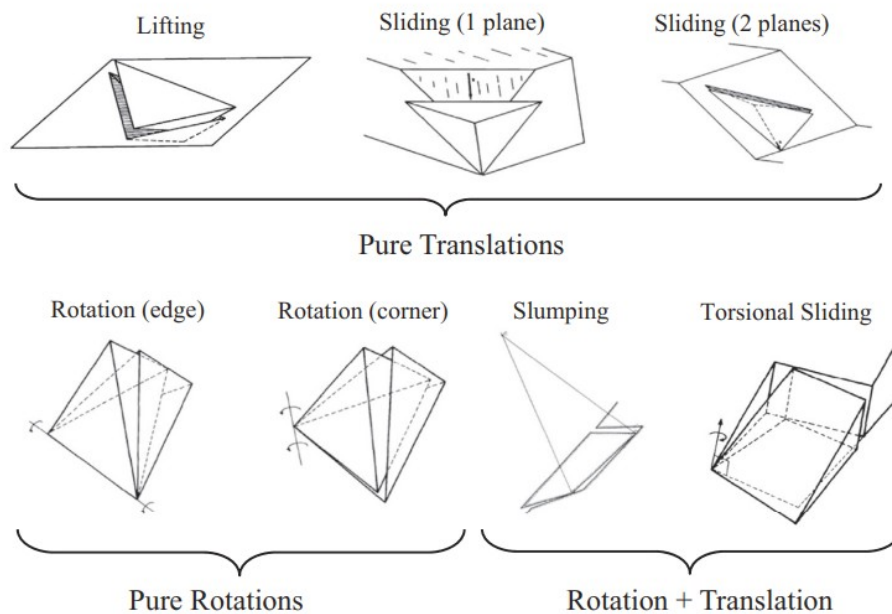**Fig. 3.** Block kinematic failure modes.[8]

For block stability, the corresponding limit equilibrium expressions for the pure translational movements[9] are below. For lifting:

$$F = |\mathbf{r}|, \tag{7}$$

for one-plane sliding:

$$F_i = |\mathbf{n}_i \times \mathbf{r}| - |\mathbf{n}_i \cdot \mathbf{r}| \cdot \tan(\phi_i), \text{ for all } i \tag{8}$$

and for two-plane sliding:

$$F_{ij} = \frac{1}{\left|\mathbf{n}_i \times \mathbf{n}_j\right|^2} \cdot \begin{bmatrix} \left|\mathbf{r}\cdot(\mathbf{n}_i \times \mathbf{n}_j)\right|\cdot\left|\mathbf{n}_i \times \mathbf{n}_j\right| - \\ \left|(\mathbf{r} \times \mathbf{n}_j)\cdot(\mathbf{n}_i \times \mathbf{n}_j)\right|\cdot \tan(\phi_i) - \\ \left|(\mathbf{r} \times \mathbf{n}_i)\cdot(\mathbf{n}_i \times \mathbf{n}_j)\right|\cdot \tan(\phi_j) \end{bmatrix}, \text{ for all } i \neq j$$

(9)

where F is the required stabilizing force applied in the direction of movement to maintain equilibrium, and ϕ_i, ϕ_j are the friction angles on joints i and j, respectively. When F is negative, the block is considered stable, and when F is positive the block is unstable. When F is zero, the block is in equilibrium such that any further increase in load will result in removal of the block.

Applied loads are incorporated into the active resultant force vector, $\mathbf{r}$, which represents a vector sum of all active forces acting on the block For rock scour purposes, these are predominantly the hydraulic pressure applied normal to the block faces and the selfweight of the block due to gravity. This can be expressed as

$$\mathbf{r} = \sum_{i=1}^{y} \frac{1}{2}\cdot\rho_w\cdot u_x^2\cdot C_{pi}\cdot A_i\cdot\mathbf{v}_i + \mathbf{W}_b$$

(10)

where ρ_w is the density of water, u_x is the mean channel flow velocity, C_{pi} is the average dynamic pressure coefficient on the ith block face, A_i is the area of the ith block face, $\mathbf{W}_b$ is the submerged weight of the block, and y is the total number of block faces. Calculation of block face area and volume can be found in Ref. 9. Information regarding average dynamic pressures around 3D rock blocks is very limited, but expressions for C_p values applied to tetrahedral blocks subject to channel flows have been determined in Ref. 11 through physical hydraulic model testing.

3. Reliability analysis: general system formulation

We use the general system reliability approach to determine the probability that scour of the rock mass will occur by failure (removal) of individual rock blocks. The state of the system in a domain, Ω, and defined by a set of n random variables, $\mathbf{x} = [x_1...x_n]$, is uniquely determined by the state of N_g components comprising the system. Each individual component, i, is represented by a limit state function (LSF), $g_i(\mathbf{x})$, and has two potential states: safe ($g_i(\mathbf{x})>0$) or fail ($g_i(\mathbf{x})\leq 0$).
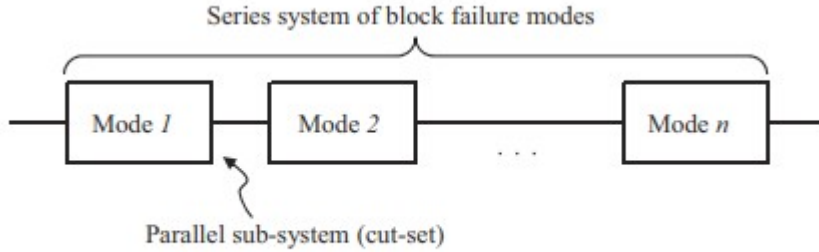
Fig. 4. Schematic for general system representation of 3D block stability.

The performance of the overall system (i.e., the stability of the block) is modeled using a minimum cut-set formulation.[12] For this purpose, the system is represented by a series assemblage of N_{cs} parallel sub-systems, or cut-sets, each of which corresponds to one of the potential kinematic modes of the block (Fig. 4). Each cut-set, C_k, is represented by a set of parallel components corresponding to the minimum criteria necessary to define failure of the block in a particular mode (i.e., the limit equilibrium and kinematic constraint expressions). A cut-set fails when all of its parallel components fail, and hence represents the intersection of component failure regions, i.e., $C_k = \cap g_i(\mathbf{x}) \leq 0$ (for $i \in C_k$) (Fig. 5). For the block, this means that 1) the equilibrium expression must indicate the block is unstable, and 2) the kinematic conditions must be met to guarantee the block can physically move in accordance with the prescribed failure mode. The overall system (block) fails when one of the cut-sets fails. Fig. 6 shows the cut-set formulation for a block subject to the pure translational modes of failure, while Table 1 lists the LSFs and their physical interpretation. For lifting mode, a limit equilibrium condition is not required, i.e., Eq. (7), as the kinematic criteria guarantee block instability when satisfied. We note that other block failure modes may be considered, such as rotation about a corner or edge, by adding other cut-sets with the appropriate expressions for stability and kinematics in series with the existing cut-sets.
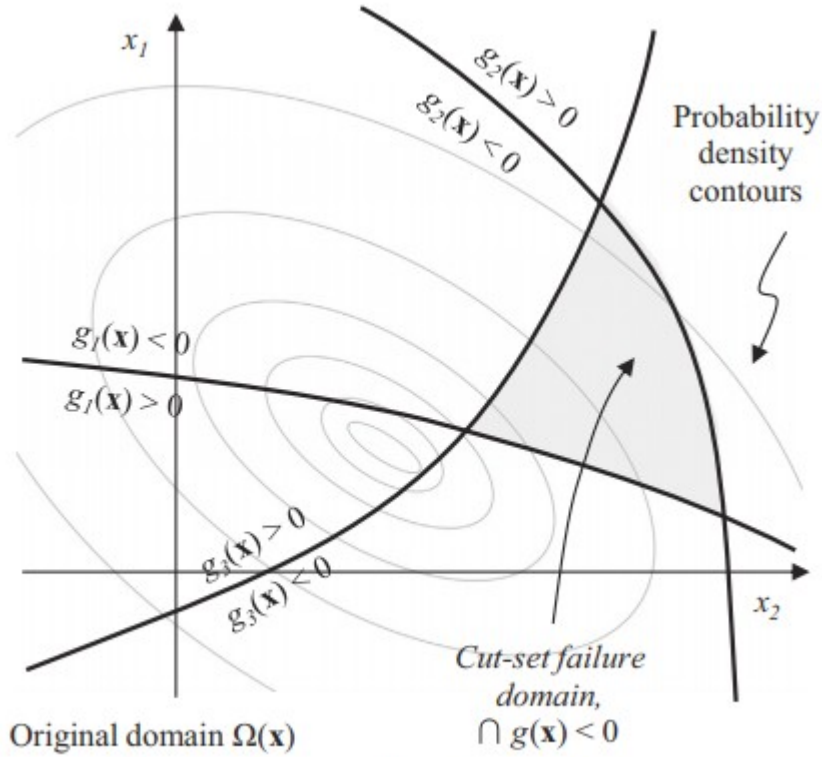
Fig. 5. Physical interpretation of cut-set (parallel system).

3.1. System failure probability

The probability of failure of a system, $P_{f,s}$, consisting of N_{cs} cutsets can be expressed as

$$P_{f,s} = P\left(\bigcup_{k=1}^{N_{cs}} C_k\right) = P\left(\bigcup_{k=1}^{N_{cs}} \bigcap_{i \in C_k} g_i(\pmb{x}) \leq 0\right),$$

(11)

which is interpreted as the probability of failure of the union of all system cut-sets. Although a number of options exist for calculating the system failure probability (including approximate methods using first order reliability method (FORM) (see, e.g., Ref. 12) and bound methods based on low-order probabilities),[13-17] we utilize the traditional Monte Carlo simulation method. Monte Carlo sampling provides an "exact" solution for the failure probability of the block system and is relatively simplistic to implement. Furthermore, discontinuous LSFs can be used which can be problematic for approximate methods like FORM. The tradeoff using Monte Carlo is increased computational effort when system failure probability is low as large numbers of samples are required to achieve a tolerable level of confidence in the failure probability value.

For Monte Carlo analysis, a set of random numbers for each of the variables, $\pmb{x}$, is generated and the system is solved deterministically N times. For each trial run an indicator function, $I(\pmb{x})$, is given a Boolean value depending on

whether failure of the block occurs (0¼safe/stable, 1¼fail/unstable). Failure probability of the system is computed by dividing the number failure occurrences by the total number of simulations:

$$I(\mathbf{x}) = \begin{cases} 1 & \text{if} \quad \overset{N_{CS}}{\underset{k=1}{\cup}} \underset{i \in C_k}{\cap} g_i(\mathbf{x}) \leq 0, \\ 0 & \text{otherwise} \end{cases} \tag{12}$$

$$P_{f,s} \cong P_{f\_MC} = \frac{1}{N} \cdot \sum_{i=1}^{N} I(\mathbf{x}_i) \tag{13}$$
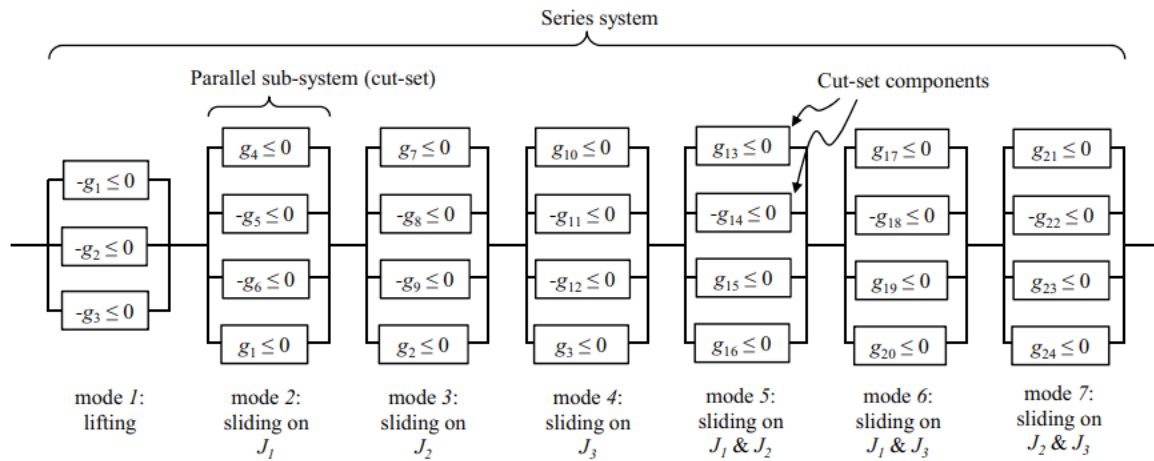

Fig. 6. Minimum cut-set formulation for 3-D block stability.

Table 1
Limit state functions for block stability model.

Failure mode	Limit state function	Physical interpretation	Eqn.
Lifting	$g_1 = \mathbf{r \cdot v_1}$	Block lifting dir. away from J1	(1)
	$g_2 = \mathbf{r \cdot v_2}$	Block lifting dir. away from J2	(1)
	$g_3 = \mathbf{r \cdot v_3}$	Block lifting dir. away from J3	(1)
Sliding on *J1*	$g_4 = -F_1$	Limit Equilibrium eqn. for sliding on J1	(8)
	$g_5 = \mathbf{s_1 \cdot v_2}$	Block sliding dir. away from J2	(4)
	$g_6 = \mathbf{s_1 \cdot v_3}$	Block sliding dir. away from J3	(4)
	g_2 (same as above)	Active resultant oriented towards J1	(1)
Sliding on *J2*	$g_7 = -F_2$	Limit Equilibrium eqn. for sliding on J2	(8)
	$g_8 = \mathbf{s_2 \cdot v_1}$	Block sliding dir. away from J1	(4)
	$g_9 = \mathbf{s_2 \cdot v_3}$	Block sliding dir. away from J3	(4)
	g_3 (same as above)	Active resultant oriented towards J2	(1)
Sliding on *J3*	$g_{10} = -F_3$	Limit Equilibrium eqn. for sliding on J3	(8)
	$g_{11} = \mathbf{s_3 \cdot v_1}$	Block sliding dir. away from J1	(4)
	$g_{12} = \mathbf{s_3 \cdot v_2}$	Block sliding dir. away from J2	(4)
	g_4 (same as above)	Active resultant oriented towards J3	(1)
Sliding on *J1* and *J2*	$g_{13} = -F_{12}$	Limit Equilibrium eqn. for sliding on J1 and J2	(9)
	$g_{14} = \mathbf{s_{12} \cdot v_3}$	Block sliding dir. away from J3	(6)
	$g_{15} = \mathbf{s_1 \cdot v_2}$	Block sliding along J1 towards J2	(6)
	$g_{16} = \mathbf{s_2 \cdot v_1}$	Block sliding along J2 towards J1	(6)
Sliding on *J1* and *J3*	$g_{17} = -F_{13}$	Limit Equilibrium eqn. for sliding on J1 and J3	(9)
	$g_{18} = \mathbf{s_{13} \cdot v_2}$	Block sliding dir. away from J2	(6)
	$g_{19} = \mathbf{s_1 \cdot v_3}$	Block sliding along J1 towards J3	(6)
	$g_{20} = \mathbf{s_3 \cdot v_1}$	Block sliding along J3 towards J1	(6)
Sliding on *J2* and *J3*	$g_{21} = -F_{23}$	Limit Equilibrium eqn. for sliding on J2 and J3	(9)
	$g_{22} = \mathbf{s_{23} \cdot v_1}$	Block sliding dir. away from J1	(6)
	$g_{23} = \mathbf{s_2 \cdot v_3}$	Block sliding along J2 towards J3	(6)
	$g_{24} = \mathbf{s_3 \cdot v_2}$	Block sliding along J3 towards J2	(6)

The total number of trails, N, is determined when the coefficient of variation of the failure probability, δ_{Pf}, is below a specified tolerance, δ_0, or when a specified maximum number of trials, N_0, is achieved. The coefficient of variation is expressed as

$$\delta_{pf} = \frac{\sqrt{N \cdot \sum_{i=1}^{N} I(\mathbf{x}_i)^2 - \left(\sum_{i=1}^{N} I(\mathbf{x}_i)\right)^2}}{\sqrt{N} \cdot \sum_{i=1}^{N} I(\mathbf{x}_i)} = \sqrt{\frac{1 - (P_{f\_MC})_i}{N \cdot (P_{f\_MC})_i}} \tag{14}$$

The individual cut-set with the highest failure probability represents the most probable block failure mode.

3.2. Parameter importance

Information regarding the relative importance of the random variables on specific system components can conveniently be obtained through FORM analysis. A key criterion for FORM requires LSFs to be continuous and differentiable to facilitate solution of a minimization algorithm to find the most probable failure point (design point) for a particular LSF (discussed in further detail below). This criterion can be relaxed for discontinuous functions, such as some of those considered in the block system formulation, as long they are continuous and differentiable in the vicinity of the design point.[12] To this end, we implement FORM to compute relative parameter importance for specific LSFs corresponding to the most probable block failure mode determined from MC analysis.

FORM utilizes a transformation of the variables, $\mathbf{x}$, and LSF, $g(\mathbf{x})$, from their original defined domain $\Omega(\mathbf{x})$ to the standard normal domain $\phi(\mathbf{u})$ where $\mathbf{u} = [u_1 \ldots u_n]$ is the vector of transformed variables, and $g(\mathbf{u})$ is the transformed LSF in the standard normal space (Fig. 7). This transformation requires knowledge of joint probability distributions between variables in the original domain, which can be difficult or impractical to obtain. As such, we assume variables are related through a Nataf distribution such that we may perform the transformation with only the information regarding their prescribed marginal distributions and correlation coefficients.[18] This is expressed as:

$$\mathbf{u} = \mathbf{L}_0^{-1} \cdot \begin{bmatrix} \Phi^{-1}\left(F_{x1}(\mathbf{x_1})\right) \\ \vdots \\ \Phi^{-1}\left(F_{xn}(\mathbf{x_n})\right) \end{bmatrix}, \tag{15}$$

where $\Phi(\cdot)$ is the univariate standard normal cumulative density function (CDF), $F_{xi}(x_i)$ is the marginal CDF of x_i, and $\mathbf{L}_0$ is the Choleski decomposition of the correlation matrix $\mathbf{R}_0$. $\mathbf{R}_0 = [\rho_{ij}]$ for $i, j = 1 \ldots n$, where ρ_{ij} is the correlation coefficient between x_i and x_j.
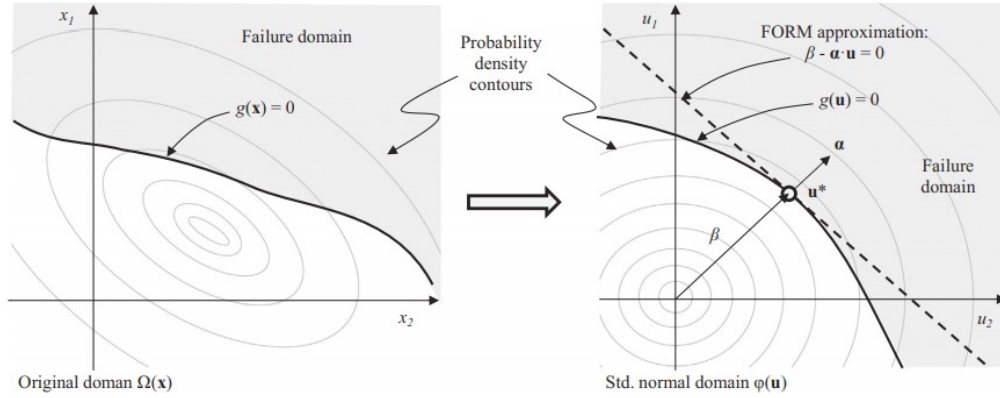
Fig. 7. First order approximation of failure probability for a component reliability problem transformed from 2D original domain (left) to 2D standard normal domain (right).

In the standard normal space, probability density contours form concentric circles around the origin (Fig. 7). The location on the LSF closest to the origin, $\mathbf{u}^*$, represents the location of maximum probability density, i.e., the point of most probable occurrence. This location is referred to as the design point and is found by solving a minimization problem using the improved Hasofer/ Lind-Rackwitz/Fiessler (iHL-RF) algorithm.[19] At $\mathbf{u}^*$, a first order (linear) approximation of the limit state function is made:

$$g(\mathbf{u}) \cong \nabla g(\mathbf{u}^*) \cdot (\mathbf{u} - \mathbf{u}^*) = |\nabla g(\mathbf{u}^*)| \cdot (\beta - \boldsymbol{\alpha} \cdot \mathbf{u}), \qquad (16)$$

where $\nabla g(\mathbf{u}^*) = [\partial g/\partial u_1 ... \partial g/\partial u_n]$ is the gradient row vector evaluated at the design point, $\boldsymbol{\alpha} = \nabla g(\mathbf{u}^*)/|\nabla g(\mathbf{u}^*)|$ is a unit vector normal to the limit state surface at the design point and $\beta = \boldsymbol{\alpha} \cdot \mathbf{u}^*$ is the reliability index. The reliability index can be viewed as an alternative measure of safety (e.g., analogous to a factor of safety in a purely deterministic problem). For statistically independent random variables, the individual terms of vector $\boldsymbol{\alpha} = [\alpha_1 ... \alpha_n]$ represent the relative importance (or contribution) of each variable, x_i, on the total variance of the linearized LSF. A larger magnitude of α_i indicates a stronger influence from x_i. A positive value of α_i signifies x_i is a demand variable and works to destabilize the system while a negative value of α_i signifies x_i is a capacity variable and works to stabilize the system. For dependent random variables, the importance vector with similar implications is represented by $\boldsymbol{\gamma}$[12]

$$\gamma = \frac{\boldsymbol{\alpha} \cdot \mathbf{J}_{x,u}^{-1} \cdot \mathbf{D}'}{\left| \boldsymbol{\alpha} \cdot \mathbf{J}_{x,u}^{-1} \cdot \mathbf{D}' \right|}, \qquad (17)$$

where $\mathbf{J}_{x,u}$ is the Jacobian matrix for the transformation from $\mathbf{x}$ to $\mathbf{u}$ space evaluated at the design point, and $\mathbf{D}'$ is the diagonal standard deviation matrix of equivalent normal random variables $\mathbf{x}' = \mathbf{x}^* + \mathbf{J}_{x,u} \cdot (\mathbf{u} - \mathbf{u}^*)$ evaluated at the design point. Note that at the design point, $\mathbf{x}' = \mathbf{x}^*$ where $\mathbf{x}^*$ is the design point in the original space.

3.3. Numerical implementation

In this work, we use the reliability code FERUM[20] developed in Matlab for Monte Carlo simulation of the failure probability of the block system, and for FORM analysis of individual system components to determine parameter importance. We modified the original Monte Carlo sampling module to include simulation for a multiple component block system.

4. Example analysis

For illustrative purposes, we present a simplified example of rock block stability under hydraulic loading using a general system reliability approach. Specifically, we examine a removable tetrahedral block in an unlined spillway bottom subject to unidirectional channel flow at a dam site in Northern California. A schematic of the spillway and block geometry is shown in Fig. 8. The authors have previously performed block theory analysis of similar blocks in a pseudo-static, deterministic sense, relating block removal to flow velocity.[11,21]
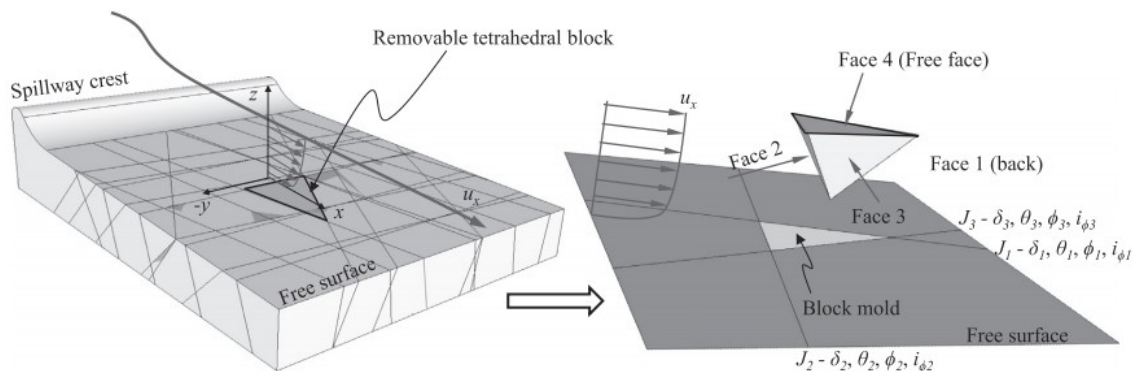

Fig. 8. Schematic of spillway and removable block geometry for reliability analysis.

4.1. Deterministic parameters, variable distributions and correlation

Joint orientations defining the block geometry (dip, δ, and dip direction, θ) were considered variable as were the friction, ϕ, and dilation, i_ϕ, angles representing the discontinuity shear strength on the block faces. The protrusion height of the block above the channel bottom, h, and the magnitude of the mean stream-wise velocity, u_x, were also considered variable. The latter two, combined with the orientation of block discontinuities, define the relative magnitude of the hydraulic pressure applied to the block faces as determined by physical testing of rock blocks subject to channel flows.[11] Flow is assumed parallel to the dip vector of the spillway surface. The orientation of the spillway channel was considered to be constant for this analysis and, therefore, was evaluated deterministically (Table 2). Other deterministic parameters are also listed in Table 2. These include the gravitational constant, g, block density, ρ_b, water density, ρ_w, parameters for pressure coefficients on block faces based on laboratory testing,[11] and the orientation of the spillway channel as defined by the dip

angle, δ_f, and dip direction, θ_f. Pressure coefficient parameters are provided for both high and low turbulence flow conditions (represented by the turbulence intensity, T_u).

Marginal distributions for all variables are presented in Table 3. For joint orientations defining the block geometry, as well as joint dilation angles, a Beta distribution was used. A Beta distribution is advantageous as variable bounds can be specified. It is also versatile in the sense that many distribution shapes can be achieved through modification of distribution parameters. For this example, distribution parameters were determined based on statistical analysis of rock mass LiDAR data collected at the dam site using SplitFX rock mass characterization software. Correlation values, ρ, between the dip and dip direction for joint sets J_1, J_2 and J_3 (also determined from LiDAR analysis) are –0.123, 0.164 and 0.135, respectively (Table 4).

Joint friction angles were also modeled using a Beta distribution. The bounds for each friction angle were assumed to range between 35° and 45° for all discontinuities. The general distribution shape was presumed to be symmetric as defined by parameters $p_1=3$, and $p_2=3$. A positive correlation $\rho=0.3$ (Table 4) was assumed between friction angles on opposing discontinuities, suggesting if a high value friction angle is observed on one joint plane, the friction angle on the other joint planes would also likely be high. Similarly, if a low value is observed on one joint plane, the values on the other joint planes would also likely be low. Note that in highly foliated or layered rock, no correlation or a negative correlation of joint friction angles may be more appropriate.

For the block protrusion height, a lognormal distribution with parameters $p_1=2$ cm and $p_2=0.5$ cm was arbitrarily selected. The protrusion height was assumed uncorrelated with the other block parameters (i.e., $\rho=0$), but inversely correlated with the flow velocity ($\rho=-0.1$). The latter implies that as the protrusion height increases the flow velocity decreases and vice versa. This is intuitive as a higher block protrusion relates to a more hydraulically rough channel which results in slower flow velocity (assuming other surface roughness asperities in the channel are of the same relative magnitude).

Normal distribution was assumed for flow velocity. The mean velocity was increased from $u_x=5$ to 10 m/s to encompass a range of conditions likely encountered at the field site. The standard deviation was determined based on hydraulic model experiments.[11] No correlation of flow velocity with other variables was assumed (except the block protrusion height as discussed above).

Table 2
Deterministic block parameters.

Parameter	Description	Value	Description
g	Gravitational constant (m/s^2)	9.81	
ρ_b	Block density (kg/m^3)	2700	
ρ_w	Water density (kg/m^3)	1000	
a	Fit parameter for C_1	0.050 (0.046)	High T_u (Low T_u) [a]
b	Fit parameter for C_1	0.901 (0.820)	High T_u (Low T_u) [a]
a	Fit parameter for C_3	0.220 (0.195)	High T_u (Low T_u) [a]
b	Fit parameter for C_3	0.333	High and Low T_u [a]
C_2	C_p correction coefficient.	0.090 (0.062)	High T_u (Low T_u) [a]
C_{pf}	C_p. on free block face	0.005	High and Low T_u [a]
δ_f	Dip angle of free surface (deg.)	10	
θ_f	Dip direction of free surface (deg.)	320	

[a] Used to determined avg. dynamic pressure coefficient (C_p) values on block faces based on expression developed from laboratory hydraulic modeling testing.[11]

Table 3

Variable statistical distributions.

Variable	Distribution	Distribution Parameters				Description
		p_1	p_2	p_3	p_4	
δ_1	Beta[a]	5.903	5.271	10	38	Dip angle J_1 (deg)
δ_2	Beta[a]	3.469	3.681	53	81	Dip angle J_2 (deg)
δ_3	Beta[a]	1.923	0.943	76	90	Dip angle J_3 (deg)
θ_1	Beta[a]	3.333	2.679	023	090	Dip direction J_1 (deg)
θ_2	Beta[a]	2.577	3.146	304	328	Dip direction J_2 (deg)
θ_3	Beta[a]	1.412	1.522	214	237	Dip direction J_3 (deg)
ϕ_1	Beta[a]	3	3	35	45	Friction angle on J_1 (deg)
ϕ_2	Beta[a]	3	3	35	45	Friction angle on J_2 (deg)
ϕ_3	Beta[a]	3	3	35	45	Friction angle on J_3 (deg)
$i_{\phi 1}$	Beta[a]	5.816	8.137	0	5.6	Dilation angle on J_1 (deg)
$i_{\phi 2}$	Beta[a]	3.926	17.927	0	14.8	Dilation angle on J_2 (deg)
$i_{\phi 3}$	Beta[a]	4.456	4.285	0	4.3	Dilation angle on J_3 (deg)
h	Log Normal[b]	2	0.5	–	–	Block protrusion height (cm)
u_x	Normal[c]	u_x[d]	$T_u \cdot u_x$[e]	–	–	Flow velocity (m/s)

[a] p_1, p_2=distribution shape parameters, p_3=a (min. value), p_4=b (max. value).
[b] p_1=λ (mean log normal space), p_2=ζ (std. dev. log normal space), p_3, p_4 not required.
[c] p_1=μ (mean), p_2=σ (std. dev.), p_3, p_4 not required.
[d] Mean value of u_x varied from 5 m/s to 10 m/s.
[e] T_u=0.06 (high T_u analysis), 0.02 (low T_u analysis).

4.2. Analysis results

Calculated failure probabilities for the block (system) and individual kinematic failure modes (sub-systems) are provided in Fig. 9 for increasing values of mean channel flow velocity for both high and low turbulence conditions. Monte Carlo simulation was performed until the coefficient of variation for the block system failure probability (calculated from Eq. (13)) was below a threshold of $\delta_{Pf}=\delta_0=0.05$ or until 10,000 trials had been performed. Note, the approximate time to perform 10,000 simulations was two hours and therefore represented a reasonable ceiling for this example study. In most cases the $\delta_{Pf}=0.05$ criterion was achieved, except when $u_x=5$ and 6 m/s. In these scenarios the analysis stopped when $\delta_{Pf}\sim0.15$ to 0.2 because of the low failure probability of the system for these two cases

($P_{f,s}$<0.005). Systems with such low failure probability would require nearly 100,000 simulations (~1 day run time) in order to reliability characterize $P_{f,s}$ to a threshold of δ_{Pf}=0.05. This highlights one of the limitations of the Monte Carlo method. The other modeled scenarios required significantly fewer simulations to achieve the threshold coefficient of variation (Table 5). Fig. 10 shows the evolution of $P_{f,s}$ and δ_{Pf} for low turbulence conditions and u_x=7 m/s.

Overall a trend of increasing block failure probability versus increasing mean channel flow velocity is witnessed, as anticipated. The failure probability begins to increase rapidly when u_x>6 m/s (high T_u) and u_x > 7 m/s (low T_u). Three failure modes are identified as the most probable to occur which include 1-plane sliding on J_3 (S3), 2-plane sliding on J_1 and J_3 (S13) and lifting (0). These are modes corresponding to the individual cut-sets with the highest failure probability. For lower mean u_x values the dominant mode is S13, while for higher u_x values S3 and 0 are more prevalent. Block removal by the other kinematic modes (S1, S2, S12, S23) yielded P_f values at or near zero indicating their unlikely occurrence.

A comparison between high and low T_u flow conditions is provided in Fig. 11. The high turbulence case shows increased block failure probability at lower flow velocities. This is attributed to greater variability in the active resultant force orientation, **r**, due to greater variability in the flow velocity, thus creating a higher probability for block instability.

Table 6 presents values of the importance vector, **γ**, for LSF g_{17} corresponding to the limit equilibrium expression for 2-plane sliding on J_1 and J_3, one of the most probable kinematic failure modes. As anticipated, individual γ values for ϕ and i_ϕ are negative indicating that friction on the joint bounding the block acts in a capacitive (stabilizing) manner. Importance values for the block joint orientations are both positive and negative. This is solely a function of block face orientation as hydraulic pressure acts normal to the block face. Depending on how the face is oriented and the failure mode under consideration, the hydraulic force on that face may work to stabilize or destabilize the block. In this example, values are predominantly positive indicating a destabilizing tendency.

As expected, γ values for block protrusion height, h, and u_x are positive indicating these variables work to destabilize the block. Interestingly, at higher flow speeds ($u_x \geq 9$ m/s) these values become negative and act in a stabilizing capacity. This corresponds with the change in dominant kinematic failure mode observed Fig. 9. At higher flow velocities, two-plane sliding on J_1 and J_3 is less relevant, while 1-plane sliding on J_3 and lifting become more probable. The increased load associated with the higher flow velocity changes the orientation of the active resultant force vector such that sliding on J_1 and J_3 becomes kinematically more difficult. This highlights the importance of kinematics in the evaluation of block stability/erodibility

Finally, examination of the relative magnitude of the importance values for each variable (i.e., |γ|) in Table 6 shows that the block protrusion height has,

by far, the most influence on block stability in this analysis ($|\gamma|\sim$0.75 to 0.95). Also of significant importance is the flow velocity ($|\gamma|\sim$0.15 to 0.20) and the orientation of the downstream block face (defined by δ_1 and θ_1) ($|\gamma|\sim$0.2 to 0.45). The magnitude of importance values for ϕ and i_ϕ representing the sliding friction are much lower than those for h, u_x, and δ_1 and θ_1. This indicates the influence of the friction angle on the stability of the block is not very significant.

Table 4
Correlation matrix, $\mathbf{R_0}$, for input variables.

	δ_1	δ_2	δ_3	θ_1	θ_2	θ_3	ϕ_1	ϕ_2	ϕ_3	$i_{\phi 1}$	$i_{\phi 2}$	$i_{\phi 3}$	h	u_x
δ_1	1													
δ_2	0	1												
δ_3	0	0	1											
θ_1	−0.123[a]	0	0	1			(symmetric)							
θ_2	0	0.164[a]	0	0	1									
θ_3	0	0	0.135[a]	0	0	1								
ϕ_1	0	0	0	0	0	0	1							
ϕ_2	0	0	0	0	0	0	0.3	1						
ϕ_3	0	0	0	0	0	0	0.3	0.3	1					
$i_{\phi 1}$	0	0	0	0	0	0	0.5	0.3	0.3	1				
$i_{\phi 2}$	0	0	0	0	0	0	0.3	0.5	0.3	0.3	1			
$i_{\phi 4b}$	0	0	0	0	0	0	0.3	0.3	0.5	0.3	0.3	1		
h	0	0	0	0	0	0	0	0	0	0	0	0	1	
u_x	0	0	0	0	0	0	0	0	0	0	0	0	−0.1	1

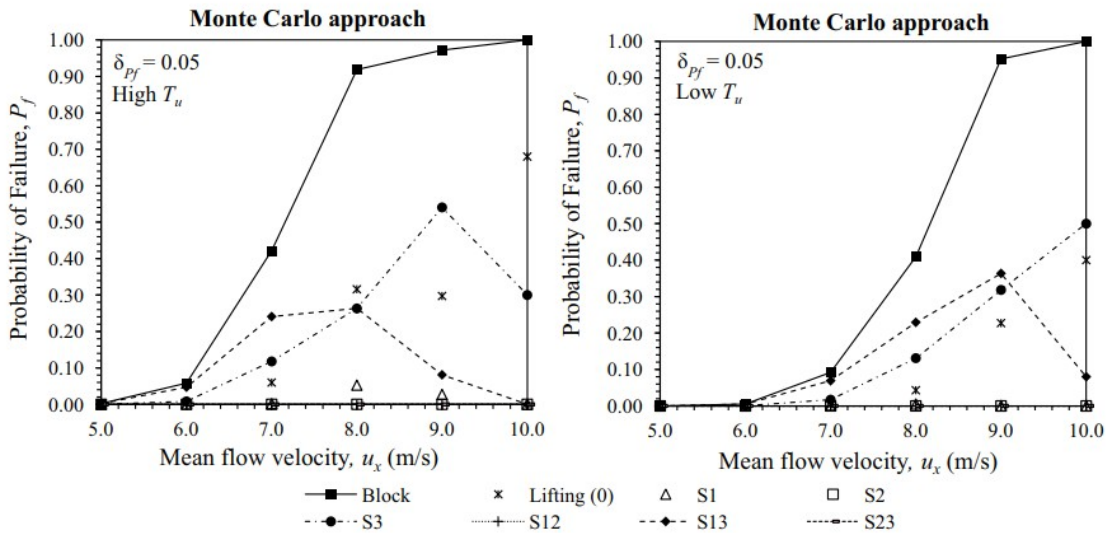[a] Correlation values, ρ, determined from analysis of site data.

Fig. 9. Monte Carlo simulation results for high (left) and low (right) T_u flow conditions.

Table 5
Monte Carlo simulation results.

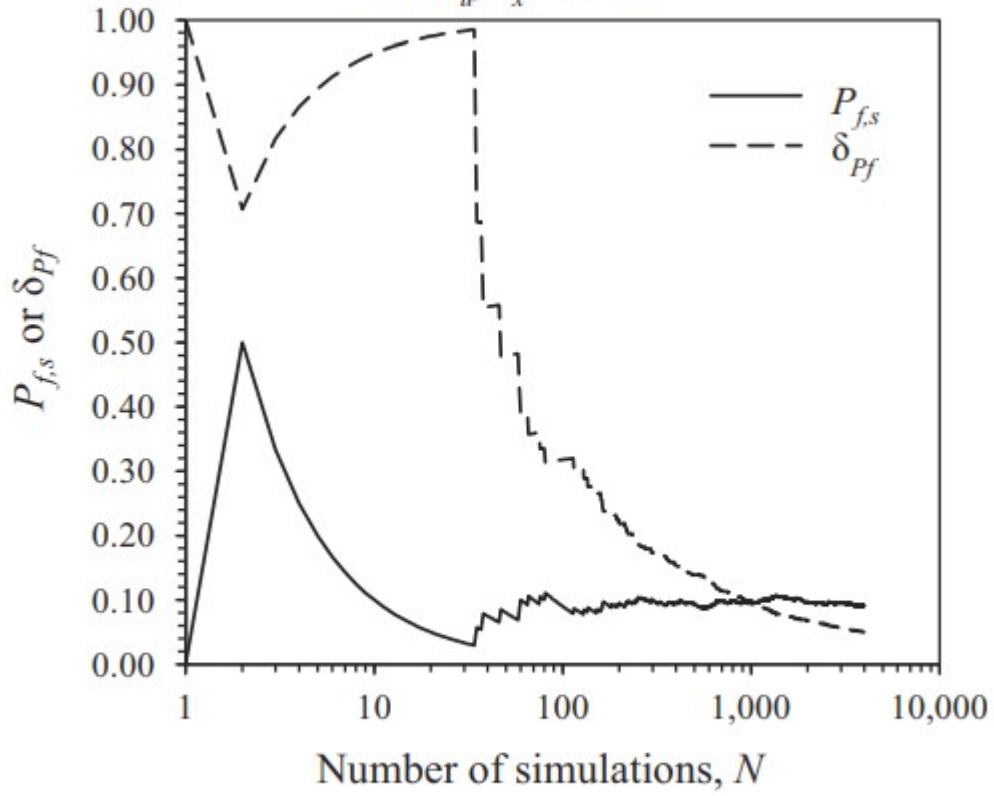| Flow velocity	Turb.	Failure probability	Coef. of var.	Number of simulations
u_x (m/s)	T_u	$P_{f,s}$	δ_{Pf}	N
5	High	0.002	0.22	10,000
6	High	0.058	0.05	6465
7	High	0.421	0.05	551
8	High	0.919	0.05	37
9	High	0.972	< 0.05	36
10	High	1.000	< 0.05	49
5	Low	0	–	10,000
6	Low	0.005	0.14	10,000
7	Low	0.092	0.05	3970
8	Low	0.409	0.05	579
9	Low	0.952	0.05	21
10	Low	1.000	< 0.05	49

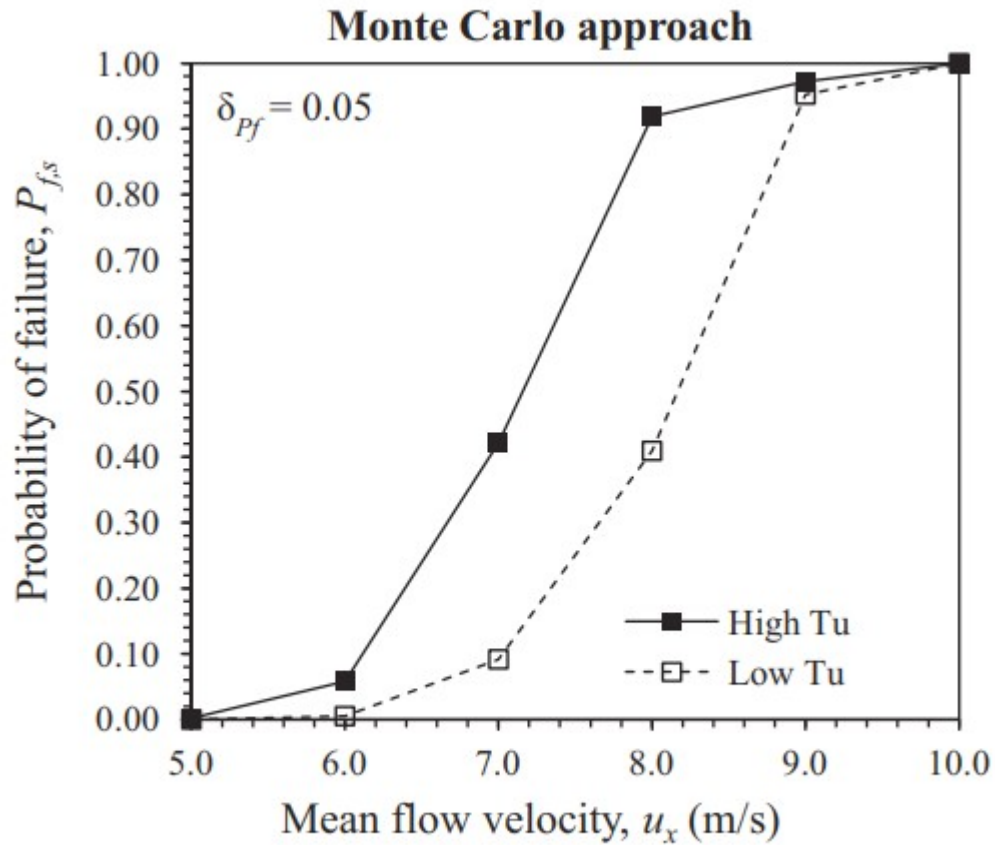**Fig. 10.** Evolution of $P_{f,s}$ and δ_{Pf} for $u_x{=}7$ m/s simulation.

Fig. 11. Comparison of block failure probability, $P_{f,s}$, for high and low T_u values.

5. Conclusions

A general system reliability approach for evaluation of 3D rock block stability within a block theory framework was developed to assess the relative influence of the key variables on the probability of block removal by hydraulic forces. We implemented a minimum cut-set formulation to assess reliability of a block "system" subject to multiple kinematic modes. This formulation was cast within the original block theory framework developed in Ref. 9 for pure translational block failure modes (i.e., lifting, one-plane sliding, and two-plane sliding). Other kinematic block modes can be readily be considered by inclusion of additional cut-sets (Figs. 4 and 6).

The reliability approach provides a convenient methodology to incorporate uncertainty associated with variables considered in 3D block stability analysis (e.g., discontinuity orientation, friction angle, hydraulic loads, etc.). Variables are described by their marginal probability density distributions and related to other variables using correlation coefficients, both of which can be determined through field and laboratory investigations. Two key outcomes of the reliability-based block stability approach include 1) block failure probability, calculated using traditional Monte Carlo simulation, and 2) parameter importance, determined using FORM. Block failure probability

information can help guide designers in decision making and risk management for key infrastructure projects, while parameter importance provides insight into the most influential variables affecting 3D block stability. The latter can be particularly useful to optimize future field or laboratory investigations to focus on variables that have the most impact on the overall system.

An example analysis using the reliability approach to evaluate 3D block erodibility is presented to incorporate variability in the analysis of the scouring process at a dam site in Northern California. The failure probability of an individual block was calculated as a function of increasing mean channel flow velocity (Fig. 9). The computed parameter importance factors show that the block protrusion height, h, is by far the most influential variable on block stability/erodibility in this example, followed by the discontinuity orientations, δ and θ, and the flow velocity, u_x (Table 6). Sliding friction, represented by the friction, ϕ, and dilation, i_ϕ, angles, is the least influential. Accordingly, from a design standpoint, future erodibility investigations would be best focused on determination of h, u_x, δ, and θ, particularly if given budgetary constraints. This highlights the usefulness of the reliability approach to systematically (and optimally) identify variables that most impact a system.

Although the focus of the present research is hydraulic loading of rock blocks in channel flow scenarios, the method can be readily applied to block stability problems of similar geometry for other loading conditions (e.g., gravity, seepage, overtopping jet) through modification of the active resultant force vector, **r**.

Acknowledgments

Table 6
Parameter importance vector, γ, when $u_x = 5$–10 m/s (low T_u).

Variable	Importance vector $(\gamma)^a$					
	$u_x = 5$ m/s	$u_x = 6$ m/s	$u_x = 7$ m/s	$u_x = 8$ m/s	$u_x = 9$ m/s	$u_x = 10$ m/s
δ_1	0.201	0.211	0.229	0.258	−0.335	−0.308
δ_2	−0.003	0.009	0.017	0.024	0.008	0.009
δ_3	0.037	0.038	0.040	0.042	−0.093	−0.078
θ_1	0.086	0.074	0.065	0.059	0.322	0.439
θ_2	0.065	0.072	0.081	0.092	−0.065	−0.074
θ_3	−0.005	0.000	0.008	0.019	−0.255	−0.318
ϕ_1	−0.035	−0.032	−0.033	−0.037	−0.067	−0.092
ϕ_2	~0	~0	~0	~0	~0	~0
ϕ_3	−0.018	−0.016	−0.016	−0.018	−0.027	−0.031
$i_{\phi1}$	−0.012	−0.011	−0.012	−0.013	−0.024	−0.032
$i_{\phi2}$	~0	~0	~0	~0	~0	~0
$i_{\phi3}$	−0.006	−0.006	−0.006	−0.006	−0.009	−0.011
h	0.961	0.958	0.950	0.935	−0.816	−0.742
u_x	0.149	0.157	0.175	0.207	−0.186	−0.196

[a] γ values provided for LSF g_{17} corresponding to the limit equilibrium equation for 2-plane sliding on J_1 and J_3).

References

1. Annandale GW. Erodibility. J Hyd Res. 1995;33:471–494.

2. Annandale GW. Scour Technology. 1st ed., New York: McGraw-Hill; 2006.

3. Bollaert E. Transient Water Pressures in Joints and Formation of Rock Scour due to High-velocity Jet Impact Switzerland: Laboratory Hyd Constructions, Ecole Polytechnique Federale de Lausanne; 2002 [Communication No. 13].

4. Jimenez-Rodriguez R, Sitar N, Chacon J. System reliability approach to rock slope stability. Int J Rock Mech Min Sci. 2006;43:847–859.

5. Low BK. Reliability analysis of rock wedges. J Geotech Geoenviron Eng. 1997;123 (6):498–505.

6. Low BK. Efficient probabilistic algorithm illustrated for a rock slope. Rock Mech Rock Eng. 2008;41(5):715–734.

7. Jimenez-Rodriguez R, Sitar N. Rock wedge stability analysis using system reliability methods. In: Proceedings of International Conference on Landslide Risk Management. Vancouver, BC; 2005, Paper J080.

8. Goodman RE. Block theory and its application. Geotechnique. 1995;45(3):383– 423.

9. Goodman RE, Shi G. Block Theory and Its Application to Rock Engineering. Englewood Cliffs, NJ: Prentice-Hall; 1985.

10. Mauldon M. Technical note: probability aspects of the removability and rotatability of tetrahedral blocks. Int J Rock Mech Min Sci. 1990;27(4):303– 307.

11. George M. 3D block erodibility: dynamics of rock-water interaction in rock scour [PhD Thesis]. Berkeley: Dept of Civil & Env Eng, Univ of California; 2015.

12. Der Kiureghian A. First- and second-order reliability methods. In: Nikolaidis E, Ghiocel DM, Singhal S, eds. Engineering Design Reliability Handbook. Boca Raton, FL: CRC Press; 2005 ch. 14.

13. Kounias EG. Bounds for the probability of a union, with applications. Am Math Stat. 1968;39(6):2154–2158.

14. Hunter D. An upper bound for the probability of a union. J Appl Probab. 1976;13:597–603.

15. Ditlevsen O. Narrow reliability bounds for structural systems. J Struct Mech. 1979;7(4):453–472.

16. Zhang YC. High-order reliability bounds for series systems and application to structural systems. Comput Struct. 1993;46(2):381–386.

17. Song J, Der Kiureghian A. Bounds on system reliability by linear programming. J Eng Mech. 2003;129(6):627–636.

18. Liu P, Der Kiureghian A. Multivariate distribution models with prescribed marginal and covariances. Prob Eng Mech. 1986;1(2):105–112.

19. Zhang Y, Der Kiureghian A. Two improved algorithms for reliability analysis. In: Rackwithz R, Augusti G, Borri A, eds. Reliability and optimization of structural systems. In: Proceedings of the 6th IFIPWG 7.5 Working Conference on Reliability and Optimization of Structural Systems. 1994, 1995: 297–304.

20. Haukaas T, Der Kiureghian A. FERUM users guide. Berkeley: Dept of Civil & Env Eng, Univ of California; 1999. ⟨www.ce.berkeley.edu/projects/ferum/⟩.

21. George MF, Sitar N. Block Theory Application to Scour Assessment of Unlined Rock Spillways. Report No. UCB GT 12-02. Berkeley: Dept of Civil & Env Eng, Univ of California; 2012.